Title: Synchrotron-X-ray fluorescence analysis reveals diagenetic alteration of fossil melanosome trace metal chemistry

Authors: Christopher S. Rogers[1,2]*, Samuel M. Webb[3], Maria E. McNamara[1,2]*

Author Affiliations:

[1]School of Biological, Earth and Environmental Sciences, University College Cork, Distillery Fields, North Mall, Cork, T23 TK30, Ireland

[2]Environmental Research Institute, University College Cork, Lee Road, Cork T23 XE10, Ireland

[3]Stanford Synchrotron Radiation Lightsource, SLAC National Accelerator Laboratory, 2575 Sand Hill Road, Menlo Park, CA 94025, USA

*Correspondence to: christopher.rogers@ucc.ie; maria.mcnamara@ucc.ie

Abstract: A key feature of the pigment melanin is its high binding affinity for trace metal ions. In modern vertebrates trace metals associated with melanosomes, melanin-rich organelles, can show tissue- and taxon-specific distribution patterns. Such signals preserve in fossil melanosomes, informing on the anatomy and phylogenetic affinities of fossil vertebrates. Fossil and modern melanosomes, however, often differ in trace metal chemistry; in particular, melanosomes from fossil vertebrate eyes are depleted in Zn and enriched in Cu relative to their extant counterparts. Whether these chemical differences are biological, or taphonomic, in origin is unknown, limiting our ability to use melanosome trace metal chemistry to test palaeobiological hypotheses. Here, we use maturation experiments on eye melanosomes from extant vertebrates and synchrotron rapid scan-X-ray fluorescence analysis

to show that thermal maturation can dramatically alter melanosome trace element chemistry. In particular, maturation of melanosomes in Cu-rich solutions results in significant depletion of Zn, likely due to low pH and competition effects with Cu. These results confirm fossil melanosome chemistry is susceptible to alteration due to variations in local chemical conditions during diagenesis. Maturation experiments can provide essential data on melanosome chemical taphonomy required for accurate interpretations of preserved chemical signatures in fossils.

Keywords: fossil, soft tissue, taphonomy, Synchrotron-X-ray fluorescence.

MELANIN is an essential biomolecule in animals that supports immunity (Agius and Roberts 2003; Nappi and Christensen 2005) and facilitates key physiological processes including directional photoreception in the eye (Oakley *et al.* 2015) and the protection of tissues from UV damage (Brenner and Hearing 2007). Melanin may also contribute to metal homeostasis via its high binding affinity for metal ions such as Ca^{+2}, Fe^{+3}, Cu^{+2} and Zn^{+2} (Hong and Simon 2007; Wogelius *et al.* 2011; Rossi *et al.* 2019) (albeit the two common forms of melanin, eumelanin and phaeomelanin, differ in metal affinity) (Wogelius et al. 2011, Manning et al. 2019). Remarkably, evidence of melanin has been reported from many vertebrate fossils, usually in association with preserved melanosomes (micron-sized organelles) (e.g. Lindgren *et al.* 2012; McNamara *et al.* 2016). As with melanin in extant animals (Hong and Simon, 2007, fossil melanin can associate with metals, especially Cu (Wogelius *et al.* 2011) and Zn (Manning et al. 2019). Preserved associations between these metals and melanosomes can be tissue- and taxon-specific (Rogers *et al.* 2019; Rossi *et al.* 2019), thus offering the potential to inform on the internal anatomy (Rossi *et al.* 2019) and

phylogenetic affinities (Rogers *et al.* 2019) of fossils and the functional evolution of melanin (Rossi *et al.* 2019).

The metal inventory of fossil melanin, however, differs from that of modern analogues, even in closely related taxa (Rossi *et al.* 2019; Rogers *et al.* 2019). In the case of vertebrate eye melanosomes, concentrations of Zn are markedly lower in fossils relative to modern vertebrate eyes, and concentrations of Cu and Fe are higher (Rogers *et al.* 2019). The origins of these differences are unclear, thus impacting our ability to confidently interpret preserved melanosome chemistry. Previous work on fossils acknowledged the possibility of diagenetic alteration of the trace metal inventory of melanosomes (Wogelius et al. 2011); this is supported by experimental evidence that the trace element chemistry of melanin is sensitive to fluctuations in pH (Hong and Simon 2007) and high metal concentrations (Chen *et al.* 2009). Characterization of the impact of diagenesis on melanosome trace metal chemistry is therefore essential to identify taphonomic biases in the melanosome fossil record.

Here, we resolved these issues by conducting maturation experiments on melanosomes from extant vertebrate eyes at elevated pressures and/or temperatures and with different chemical media in order to simulate how different pore fluids (i.e. sources of metal ions) interact with melanosomes during diagenesis. Analysis of the results using synchrotron rapid scan-X-ray fluorescence analysis (SRS-XRF) and X-ray absorption spectroscopy (XAS) reveals which melanosome-associated elements are susceptible to changes in concentration during diagenesis. Critically, the experimental data aid interpretations of the chemical differences between fossil and modern eye melanosomes, thus informing on key biases in the melanosome fossil record.

MATERIALS and METHODS

Modern specimens

Specimens of European sea bass (*Dicentrarchus labrax* n = 14) were obtained from commercial suppliers and dissected within 24 h after death. One eye from each animal was bisected and melanin was enzymatically extracted from the posterior half of each eye (including the melanosome-rich choroid and retinal pigment epithelium (RPE)) using the method in Rossi *et al.* (2019). The extraction process breaks down cellular material and can degrade phaeomelanin, yielding extracts that are biased towards eumelanin (Liu et al. 2005).

Fossil specimens

Preserved melanosomes from the eyespot of a specimen of *Dapalis macrurus* (CKGM F 6 427; Actinopterygii: Perciformes, from Alpes de Haute-Provence, France (Oligocene)) and eyespots from the fossil teleosts Tetradontiformes indet. (NHMD 199 838; from the Fur Formation, Denmark (Eocene)) and *Knightia* (FOBU 17 591; Actinopterygii: Clupeiformes from the Fossil Butte member of the Green River formation, Colorado/Utah/Wyoming (Eocene)) were reported in Rogers *et al.* (2019) and analyzed further as below.

The respective fossil localities vary in lithology and diagenetic history. NHMD 199 838 is hosted in diatomite that was deposited in a restricted marine basin (Pedersen and Buchardt, 1996) and experienced at least 40–45°C and ~33–49 bar during diagenesis (McNamara et al. 2013). FOBU 17 591 is hosted in laminated limestone that was deposited in a restricted terrestrial basin with marked salinity fluctuations during deposition (Loewen and Buchheim 1998). Data on diagenetic history are not available for the Fossil Butte Member (part of the Fossil Basin); sediments from the Uinta Basin of the Green River Formation experienced

burial conditions of up to 65–180°C and ~400–2000 bar (McNamara et al. 2013). CKGM F 6427 is preserved in a laminated limestone but lacks stratigraphic data; specimens of this taxon are common in the freshwater/brackish lacustrine limestones of the Campagne-Calavon Formation of Alpes de Haute-Provence (Gaudant, 2015), though data on burial history are not available.

Institutional abbreviations: NHMD, Natural History Museum of Denmark; CKGM, Cork Geological Museum at University College Cork; FOBU, Fossil Butte National Monument.

EDTA treatment of melanin

Unmatured melanin (50–100 mg) extracted from a single *Dicentrarchus* eye was added to an aqueous solution of EDTA (one ml) for 24 h at room temperature and then centrifuged. This process was repeated six times followed by washing four times in biomolecular-grade water in order to remove excess EDTA. The EDTA-treated extract was then added to one ml of 16 mmol Cu-solution for 24 h at room temperature before being washed twice in 10^{-3} M HCl to precipitate any Cu still in solution (Hong *et al.* 2004). The extract was washed twice in biomolecular water and once in acetone. Half of the extract was experimentally matured (see below).

Experimental maturation

Taphonomic studies investigating the impact of maturation on soft tissues typically use elevated temperatures and pressures for relatively short periods of time (usually < 24 h) to artificially simulate aspects of the maturation process (McNamara *et al.* 2013; Colleary *et al.* 2015). Such experiments are known to yield morphological and chemical phenomena similar to those exhibited by fossils (Stankiewicz *et al.* 2000). Melanosome extracts for experimental

maturation (n = 12) were each inserted into separate Au capsules. To each capsule was added one ml of experimental medium, defined as follows. The EDTA-treated extract used distilled deionized (DD) water. All other extracts used either DD water, “Cu-solution” (Trace Cert Copper standard for AAS (1 000 mg l^{-1})), “Zn-solution” (Trace Cert Zinc standard for AAS (1 000 mg l^{-1})) or “Cu-Zn-solution” (50:50 mixture of Trace Cert Copper and Zinc standards for AAS (Rogers et al. 2020 (Table S1))). The inclusion of metal ion solution in some experiments is designed to test how variation in diagenetic pore fluid chemistry impacts melanin chemistry. All metal ion solutions have a concentration of 16 mmol and are at pH 3.

Brushes were used to remove any extract or experimental medium from the termini of each capsule prior to them being welded shut with a Lampert PUK 4 microwelding system. Sealed capsules were thermally matured for 24 h at 200°C in either an oven at one bar or, for some samples (including EDTA-treated extracts) a custom-built high-pressure high-temperature rig (StrataTech, UK) at 120 bar. It was not possible to measure the pH of the experimental medium at the end of the experiment due to the small size of the capsules and unpredictable escape of fluid from the capsules upon opening.

Synchrotron Rapid Scanning-X-ray Fluorescence (SRS-XRF) analysis

X-ray fluorescence spectra were collected from matured and untreated extracts and fossils at beamline 2-3 at the Stanford Synchrotron Radiation Lightsource (SSRL). Extracts and small samples (ca. one mm^2) of dark brown carbonaceous material from the eyespot of the fossil fish *Dapalis macrurus* (Oligocene, CKGM F 6 427) were mounted on kapton tape. Samples were spatially rastered by a microfocused beam of two μm^2 provided by an Rh-coated Kirkpatrick-Baez mirror pair with 20–50 ms/pixel dwell time. A Si (111) double crystal monochromator was used to set incident X-ray energy at 11 keV; the storage ring was in top-

147 off mode at three GeV and contained 500 mA. Samples were mounted at 45° to the incident
148 X-ray and the intensity of the beam was measured using a nitrogen-filled ion chamber. At
149 each data point, the intensity of fluorescence lines for selected elements (P, S, Ca, Ti, Mn, Fe,
150 Ni, Cu and Zn) was collected and monitored using an Xpsress3 pulse processing system
151 (Quantum Detectors) coupled to a silicon drift Vortex detector (Hitachi, USA) for energy
152 discrimination.
153
154 *SRS-XRF data processing*
155 MicroAnalysis Toolkit software (Webb 2011) was used to normalize fluorescence spectra
156 and calibrate concentrations of each element in μg/cm^2 against NIST traceable thin-film
157 elemental standards. Mean concentrations and standard deviation values for each element
158 were calculated for selected regions of interest. Inspection of SRS-XRF spectra from the
159 Multi-Channel Analyzer (MCA) data reveals that in extracts the concentrations of certain
160 elements (P, S, Ti and Mn) are too low to be discriminated confidently from the background
161 (Rogers et al. 2020 (Figs S1–S7)). Concentration data from these elements were therefore
162 excluded from further analyses. Ni was identified in the MCA data but concentrations (< nine
163 μg/cm^2) were markedly lower than those of other elements and thus Ni was also excluded
164 from further analysis.
165
166 The SRS-XRF data were analyzed further using Linear Discriminant Analysis (LDA) in
167 PAST (Hammer *et al.* 2001) to visualize variations in the chemistry of selected elements (Ca,
168 Fe, Cu and Zn) among the melanin extracts and fossil melanosomes. The significance of
169 differences in concentration among samples was assessed using ANOVA or non-parametric
170 alternatives (Kruskal-Wallis and Welch's F-test) and appropriate pairwise post hoc analyses

(Tukey, Mann Whitney and Dunn, respectively). Differences in elemental concentrations among extracts were visualized using box plots.

X-ray absorption spectroscopy (XAS)

EDTA-treated extracts and samples from the eyespot of *Dapalis* were mapped at beamlines 2-3 and 10-2 at the Stanford Synchrotron Radiation Lightsource (SSRL). At beamline 2-3 extracts were analyzed as above. At beamline 10-2 extracts were analyzed using a 25–200 μm beam using a series of tungsten apertures. Four to six points of interest were selected from each SRS-XRF map. XAS spectra were collected from these points by driving the emitted intensity from ~8 787 eV to ~9 827 eV across the Cu K edge (set at 8 987 eV using a Cu foil) in a stepwise fashion (step size of 10 eV from 8 749 to 8 958 eV, except for between 8 959 to 9 006 eV (i.e. across the Cu K edge) where step size of 0.35 eV was used. Between two and seven repeat scans (15 min each) were collected at each point.

A Cu foil was used to calibrate the energy of the monochromator. X-ray absorption near edge structure spectroscopy (XANES) was used to investigate the oxidation state of Cu associated with the melanosomes in our dataset. Each spectrum was monitored for loss of intensity and photo-reduction associated with exposure to the electron beam. No evidence for photo-reduction was observed among replicate scans and repeat scans at each point are mutually consistent. Spectra were processed as standard (i.e. via normalization and background removal) in Athena (Ravel and Newville 2005).

RESULTS

Trace metal concentrations in matured melanosome extracts

Linear Discriminant Analysis (LDA) plots of the SRS-XRF data show extensive overlap of data from unmatured and matured melanosomes in chemospace (Fig. 1A–B). Differences in trace element chemistry between untreated extracts and extracts experimentally matured in DD water are not statistically significant (*p-values*=0.1034–0.8206, Rogers et al. 2020 (Table S2A–C)); these two samples cannot therefore be distinguished chemically.

Concentrations of Ca (Welch F: df = 16.18, F = 73.39, p = 7.91^{-11}) and Cu (df = 17.47, F = 118.8, p = 5.792^{-13}) are significantly different between unmatured extracts and extracts matured in Cu and/or Zn-solutions (Fig. 2, Rogers et al. 2020 (Table S2A)). More specifically, concentrations of Ca are significantly lower in extracts matured in Zn-solution and mixed Cu-Zn-solution (Dunn's post hoc p = 0.002–0.006). Concentrations of Cu are higher in extracts matured in Cu-solution and mixed Cu-Zn-solution (p = 0.001–0.002) (Rogers et al. 2020 (Table S2B–C)). Concentrations of Zn are significantly lower in all extracts matured with Cu- and/or Zn-solution (Kruskal-Wallis H (chi^2) = 23.33, p = 0.001; Dunn's post hoc p = 0.001–0.006). Variations in Fe concentrations among untreated and experimentally matured extracts are not significant (ANOVA df = 2.115, F = 17.5, p = 0.1034).

Comparison with fossil trace element chemistry

The principal component analysis plot of the fossil data reveals that the eyespot data for individual specimens plot close to the data for the associated host sediment (Figure S9); the data for individual specimens and their sediment do not overlap with those for other fossils. Variation in concentrations of Ca, Fe and Cu among specimens are significantly different

(Ca: Welch F: df = 2.668, F = 37.62, p = 0.01109; Fe: ANOVA: df = 8, F= 162, p = 6.01^{-06}; Cu: Welch F: df = 2.983, F = 13.7, p = 0.03136; posthoc tests: Rogers et al. 2020 (Table S4)). Concentrations of Zn do not differ significantly among specimens (Kruskal-Wallis H (chi^2) = 0.3556, p = 0.8371).

Differences in concentrations of Cu between the fossil eyespots and the host sediment are significantly different for each fossil specimen (Rogers et al. 2020 (Table S4)). In addition, concentrations of Fe (and, in *Dapalis*, Ca) are significantly different between the eyespot of *Knightia* and the respective host sediment; similarly, concentrations of Fe and Ca differ significantly between the eye of *Dapalis* and the host sediment. Differences in concentrations of Zn between eyespots and host sediment are not significantly different for any of the three fossils analyzed (Rogers et al. 2020 (table S4)).

LDA plots of the total dataset reveal three major groupings in the LDA chemospace (Fig. 3A): (1) fossil melanosomes, (2) melanosome extracts matured in Cu-solution and Cu-Zn-solution, and (3) melanosome extracts matured in DD water, in Zn-solution and untreated melanosomes. The primary elements driving this chemical variation are Ca, Cu and Zn (Fig. 3B); in particular, fossil melanosomes have significantly lower concentrations of Zn than untreated modern equivalents (Kruskal-Wallis (H (chi^2) = 12.79, 0.0003). Fossil and untreated modern melanosomes do not differ significantly in concentrations of Ca (Kruskal-Wallis H (chi^2) = 1.421, p = 0.233)), Cu (H (chi^2) = 0.002, p = 0.965)) or Fe (F = (1, 16) = 3.478, p = 0.081) (Rogers et al. 2020 (Table S5)). In the total dataset, however, differences in Cu concentrations between samples are significant (Kruskal-Wallis (H (chi^2) = 7.2, 0.02732); differences in concentrations of Ca (Kruskal-Wallis (H (chi^2) = 5.422, 0.06646), Fe (Kruskal-

242 Wallis (H (chi^2) = 5.6, 0.06081) and Zn (Kruskal-Wallis (H (chi^2) = 0.3556, 0.8371) are not
243 significant.

244

245 Cu-XANES spectra for all samples analyzed have a dominant peak centred at 8 997.5 ±1 eV
246 showing a major contribution from Cu(II) (Fig. 3C). Only the Cu-XANES profile from the
247 eyespot of *D. macrurus* shows a distinct pre-edge feature at 8 984.5 eV, indicating a
248 contribution from Cu(I).

249

250 **DISCUSSION**

251 The results of our study reveal that the metal inventory of eye melanosomes is not
252 significantly altered by maturation in DD water (Fig. 1A–B). This suggests that melanosome-
253 metal associations should persist in natural diagenetic scenarios where pore fluids have low
254 concentrations of metal ions and, since pH decreases with increasing temperature, where pH
255 does not vary markedly. In contrast, melanosome extracts matured in Cu and/or Zn solutions
256 differ in chemistry to untreated samples, and to each other. This confirms that the metal
257 inventory of melanosomes is highly sensitive to local ionic concentrations during diagenesis.

258

259 Metals commonly bind to three functional groups within the eumelanin molecule (OH^-, NH_4^+
260 and $COOH^-$) (Hong *et al.* 2004); Cu can also be accommodated within the eumelanin
261 porphyrin structure, which may survive diagenesis in at least some fossils (Wogelius *et al.*
262 2011). In *Sepia* melanin, Fe(III) can bind to NH_4^+ or OH^- (Hong *et al.* 2004); Ca(II) and
263 Zn(II) bind to $COOH^-$ and Cu(II) binds primarily to OH^-. In all cases eumelanin-bound
264 metals are strictly co-ordinated to light elements (i.e., O/N). Unlike eumelanin, phaeomelanin

comprises monomers (benzothiazine and benzothiazole) that contain S and can chelate Zn (Manning et al. 2019); whether the phaeomelanin S-groups (and other groups present, e.g. NH^-) commonly bind other metals is unclear.

Extracts matured in Cu-solution are enriched in Cu and depleted in Zn relative to unmatured melanosomes. Experiments at room temperature and pressure indicate that where Cu concentrations exceed 10 mmol, additional Cu(II) can bind to $COOH^-$ sites normally occupied by Ca(II) and Zn(II) (Hong and Simon 2006), displacing the latter two elements. This is consistent with evidence of Cu-binding to melanin $COOH^-$ groups in fossil feathers (Wogelius *et al.* 2011). In our experiments it is possible that the concentration of the Cu-solutions used (16 mmol) was sufficiently high to trigger replacement of Zn(II) by Cu(II) at $COOH^-$ sites during maturation. Experiments on artificial eumelanin, however, show a decrease in $COOH^-$ with thermal maturation (Ito *et al.* 2013). Elevated Cu concentrations in our experiments may therefore reflect (at least in part) the binding of Cu to unoccupied OH^- or NH_4^+ rather than $COOH^-$.

Surprisingly, Zn concentrations decrease even when melanosome extracts are matured in solutions containing Zn. Following saturation of $COOH^-$ groups with Zn(II), NH_4^+ and OH^- groups can present secondary binding sites for Zn(II) (Hong and Simon 2006). Melanin, however, has a much higher overall binding affinity for Cu(II) than for Zn(II) (Hong and Simon 2007) and thus Zn(II) may be unable to bind to OH^- groups in melanin when they are already occupied by Cu(II). Low Zn concentrations in melanosomes matured in Cu-Zn-solutions may therefore reflect the following: (1) saturation of OH^- groups by Cu(II) from the experimental medium and the inability of Zn(II) to displace melanin-bound Cu(II) at these

289 sites, and (2) a decrease in the abundance of $COOH^-$ bonds due to thermal maturation (Ito *et*
290 *al.* 2013).

291

292 The decrease in Zn concentrations in melanosomes matured in Zn-solutions (i.e., where
293 saturation of OH^- groups by Cu(II) cannot occur, as in experiments with Cu-solution) is also
294 consistent with a maturation-induced decrease in available $COOH^-$ (Ito *et al.* 2013). This
295 indicates that the original $COOH^-$-Zn bond present in the untreated extracts was unstable
296 under the conditions used in our experiments.

297

298 Concentrations of Fe do not differ among untreated and treated melanosomes. This is
299 somewhat surprising because melanin has a higher affinity for Cu(II) than Fe(III) (Hong and
300 Simon, 2007) and thus Cu(II) may be expected to replace Fe(III) at the OH^- group (to which
301 Cu commonly binds (Hong and Simon 2007)) and the NH_4^+ group (to which it binds when
302 present in concentrations <10 mmol (Hong and Simon 2006)). Instead, our data suggest that
303 the additional Cu(II) has not displaced Fe(III) at OH^- and NH_4^+ groups but is bound
304 elsewhere, either to unoccupied functional groups or to $COOH^-$ groups in which Cu(II)
305 replaces previously bound metals such as Zn(II).

306

307 Patterns of Ca enrichment and depletion in our dataset are complex. Relative to untreated
308 samples, melanosome extracts are depleted in Ca when matured in Zn and Cu-Zn-solutions
309 but concentrations of Ca are the same when extracts are matured in Cu-solution (Fig. 2). This
310 may reflect changes in pH during the experiments. Metal binding sites in *Sepia* melanin are
311 sensitive to changes in pH; more specifically, increased acidity (e.g. a change from pH 7 to

pH 2) results in a decrease in the concentration of elements bound to $COOH^-$ groups (Liu *et al.* 2004). This reflects protonation of $COOH^-$ groups by H^+ and associated replacement of chelated metals such as Ca(II) (Liu *et al.* 2004). The exact reasons why this occurs in melanosome extracts matured with Zn and Cu-Zn-solutions but not in extracts matured only in Cu solutions is unclear but it may reflect differences in temporal changes in pH evolution in different experimental settings.

The suspension of melanin in low pH Cu- and/or Zn-solutions in our experiments may have resulted in the replacement of $COOH^-$-bound Ca(II) and Zn(II) by H^+. This process cannot, however, explain the high Ca concentrations in extracts matured in Cu-solution, the origin of which remains unclear. The persistence of Ca(II) in thermally matured samples implies either the survival of some $COOH^-$ groups under conditions understood to induce decarboxylation (Ito *et al.* 2013) or binding of Ca(II) to other functional groups in melanin or associated proteins within the melanosome. It is possible that the Ca signal could reflect contributions from other recalcitrant tissue components of the eye, but this is unlikely given that the extracts comprise near-pure agglomerations of melanosomes.

Our experiments provide an empirical basis for interpreting the chemistry of fossil melanosomes and, in particular, can help us interpret key chemical differences between these and modern melanosomes. Differences in chemistry between the fossil specimens studied may reflect taxonomic or biota-level differences; the small sample size prevents discrimination of these interpretations. Given other evidence for pervasive biota-level control on fossil melanosome chemistry (Rossi et al., 2020), the chemical differences among the specimens in this study likely represent a sedimentary signal (Rogers et al. 2020 (Fig. S9)).

The consistent offset in the chemical data for eyespots (especially enrichment of Cu) relative to the host sediment could indicate retention of a component of original chemistry (i.e. naturally elevated concentrations of Cu similar to those *in vivo*) or concentration of elements, especially Cu, in fossil melanosomes during diagenesis.

Direct comparison of the fossil and experimental data reveal that both fossil and thermally matured melanosomes are strongly depleted in Zn relative to unmatured samples. This supports our experimental data on Zn mobility during diagenesis and suggests that the Zn concentrations in the fossils are not original but likely lower than *in vivo*. In natural settings, any Zn(II) displaced as a result of a decrease in pH is likely to be mobilized and lost from the system. Alternatively, displaced Zn may be rendered unavailable for re-chelation by fossil melanin via incorporation into inorganic mineral precipitates in the host sediment.

A decrease in pH could occur relatively early *postmortem* via the release of organic acids during decay (Briggs and Kear 1993) or through contact with pore waters rich in H^+ ions. Higher temperatures at deeper burial conditions would also lower pH, further promoting the loss of Zn from fossil melanosomes. Degradation of phaeomelanin (and loss of key Zn binding sites including S^{2-} and OH^- (Manning *et al.* 2019)) during diagenesis could lead to a further depletion of Zn. This process is unlikely to contribute significantly to our experimental data, however, as the eye melanin of *D. labrax* is dominated by eumelanin *in vivo* (Rogers *et al.* 2019) and most or all phaeomelanin originally present in the tissue is likely to have been degraded during enzymatic extraction (Liu *et al.* 2005). Uplift and exposure would presumably result in an increase in local pH, but it is unclear whether thermally altered melanin could bind available Zn in this scenario, especially given that

thermal maturation is associated with decarboxylation of melanin (Ito *et al.* 2013) and thus loss of preferred functional groups for Zn-melanin chelation.

Ca, Fe and Cu concentrations are similar in fossil melanosomes and unmatured extracts. This suggests that original associations between Ca(II), Fe(III) and Cu(II) and melanin may have been retained. Melanin, however, has a lower binding affinity for Ca(II) than Zn(II) (Hong and Simon 2007); given that Zn was lost from matured melanosomes in our experiments it thus seems unlikely that original associations between Ca(II) and melanin would survive diagenesis. Instead, it is plausible that Ca concentrations in the matured melanosome extracts may reflect loss early during diagenesis and subsequent re-binding of Ca(II) once local pH and ionic conditions become more favourable. This suggests that the melanin molecule may retain a dynamic relationship with its environment long into diagenesis. Other metals such as Fe and Cu, originally bound to melanin, could also be lost and rebound in this fashion. Alternatively, some Ca, Fe and Cu associated with fossil eye melanosomes may have been bound to non-melanin labile organic components *in vivo*. Breakdown of those compounds during diagenesis and subsequent incorporation of metal ions into remnants of the melanin molecule (Wogelius *et al.* 2011) could contribute to concentrations of these metals in fossil melanosomes, but this hypothesis requires testing. Although biomolecules are understood to undergo the loss of functional groups during diagenesis (Eglingtonet al. 1991, Ito *et al.* 2013), our results suggest at least some of these functional groups must survive this process and remain viable binding sites for various metal ions.

Application of these SRS-XRF data to fossils strongly suggests that low Zn concentrations and low Zn: Cu ratios in some fossil vertebrate eye melanosomes are a diagenetic artefact

(Fig. 4). Our previous study revealed that eye melanosomes in fossil vertebrates have low Zn relative to extant analogues (Rogers et al. 2019). Our experimental data reveal that this likely reflects the loss of Zn and/or the replacement of Zn by Cu during diagenesis. Variation in the chemistry of melanosomes preserved in fossils from different biotas likely reflects different ionic concentrations, pH and burial regimes during diagenesis (Rogers *et al.* 2019). Variation in diagenetic regime, however, is less likely to explain spatial heterogeneity in melanin chemistry within a single fossil. In the latter scenario chemical variation is more likely to reflect biological factors, e.g. original variation in eu- and phaeomelanin content due to integumentary patterning (Wogelius et al. 2011) and/or enrichment in various internal organs (Rossi et al. 2019, 2020). Higher concentrations in some fossil vertebrates, especially those hosted within concretions (such as those from the Mazon Creek), may reflect rapid cementation of the host sediment, limiting interactions of pore fluids with melanosomes (and thus loss of Cu and Zn) later during diagenesis.

Cu-XANES spectra for matured and untreated melanosomes are dominated by signals for Cu(II). The local binding environment of melanosomal Cu clearly does not alter substantially during maturation (Fig. 3C). The presence of a Cu(I) signal in fossil melanosomes from *Dapalis* could reflect an artefact of the XANES analysis whereby some Cu(II) was reduced during analysis. Other vertebrate fossils (Wogelius *et al.* 2011; Rogers *et al.* 2019) and modern melanosomes analyzed under identical conditions, however, do not show a contribution from Cu(I). Instead, the Cu(I) contribution to the *Dapalis* XANES spectrum may be a real signal, reflecting local conditions during diagenesis.

In conclusion, our study reveals the effects of diagenesis on trace element chemistry of melanosomes. Specifically, our data confirm that relatively low concentrations of Zn in fossil vertebrate eye melanosomes is likely to be a diagenetic feature and that this depletion in Zn relative to modern eye melanosomes is controlled, in large part, by local ionic and pH conditions during diagenesis and not by elevated temperatures and pressures alone. Our experiments also show that original concentrations of Ca and Cu in melanosomes are susceptible to changes during maturation. The fossils we studied show considerable variation in the concentrations of Ca and Cu, likely due to variations in the diagenetic history of the deposit. Our data also reveal that the oxidation state of Cu is not altered under conditions of our maturation experiments, but that it may be altered during fossilization. These results confirm that components of the preserved trace element chemistry of fossil melanosomes could be a diagenetic artefact and that maturation experiments can yield essential insights into the chemical taphonomy of melanosomes that should be incorporated into future interpretations of preserved chemical signatures in fossils.

Collectively, our data emphasise the dynamic nature of links between fossil chemistry and the host sediment, in particular variations in pore fluid chemistry, through time. Melanin elemental chemistry is clearly plastic during diagenesis. Other, more labile, components of fossil chemistry, e.g. proteins (Asara et al. 2007, Schweitzer et al. 2007, Schweitzer et al. 2013, Schroeter et al. 2017) and nucleic acids (Schweitzer et al. 2013, Bailleul et al. 2020), would presumably be equally, if not more, susceptible to alteration during decay and diagenesis.

Acknowledgements. We thank Nick Edwards and Sharon Bone for XAS and XRF support, T. Clements, T. Slater, V. Rossi for help with XAS and XRF data acquisition and helpful discussion. Supported by European Research Starting Grant (grant no. ERC-2014-StG-637691-ANICOLEVO) awarded to M.E.M. The use of the Stanford Synchrotron Radiation Lightsource, SLAC National Accelerator Laboratory, is supported by the US Department of Energy, Office of Science, Office of Basic Energy Sciences under contract no. DE-AC02-76SF00515 via beamtime proposals 4615 and 5072 awarded to M.E.M.

Author contributions. M.E.M. and C.S.R. conceived the study; C.S.R., M.E.M. and S.M.W. performed synchrotron rapid scanning-X-ray fluorescence and X-ray absorption spectroscopy (XAS); C.S.R. and M.E.M. wrote the manuscript with input from S.M.W.

Supplementary data. All data is provided in the main text or via the Dryad Digital Repository:
https://datadryad.org/stash/share/H5aMNvcCsDvpSa94b2Wf8T69ZSdwlLc3Cb9zMAI0hn4.

References:

AGIUS, C. and ROBERTS, R. J. 2003. Melano-macrophage centres and their role in fish pathology. *Journal of Fish Diseases*, **26**, 499–509.

ASARA, J. M., SCHWEITZER, M. H., FREIMARK, L. M., PHILLIPS, M. and CANTLEY, C. L. 2007. Protein sequences from mastodon and *Tyrannosaurus rex* revealed by mass spectrometry. *Science*, **316**, 280–285.

BAILLEUL, A. M., ZHENG, W., HORNER, J. R., HALL, B. K., HOLLIDAY, C. M. and SCHWEITZER, M. H. 2020. Evidence of proteins, chromosomes and chemical markers of DNA in exceptionally preserved dinosaur cartilage. *National Science Review*, **7**, 815–822.

BRENNER, M. and HEARING, V. J. 2007. The protective role of melanin against UV damage in human skin. *Photochemistry and Photobiology,* **84**, 539–549.

BRIGGS, D. E. G. and KEAR, A. J. 1993. Fossilization of soft tissue in the laboratory. *Science*, **259**, 1439–1442.

CHEN, S., XUE, C., WANG, J., FENG, H., WANG, Y., MA, Q. and WANG, D. 2009. Adsorption of Pb(II) and Cd(II) by squid *Ommastrephes bartrami* melanin. *Bioinorganic Chemistry and Applications,* **2009**, 901563.

COLLEARY, C., DOLOCAN, A., GARDNER, J., SINGH, S., WUTTKE, M., RABENSTEIN, R., HABERSETZER, J., SCHAAL, S., FESEHA, M., CLEMENS, M. and JACOBS, B. F., CURRANO, E. D., JACOBS, L. L.,LYNG SYLVESTERSEN, R., GABBOTT, S. E. and VINTHER, J. 2015. Chemical, experimental and morphological evidence for diagenetically altered melanin in exceptionally preserved fossils. *Proceedings of the National Academy of Sciences USA*, **112**, 12592–12597.

EGLINGTON, G. and LOGAN, G. A. 1991. Molecular preservation. *Philosophical Transactions of the Royal Society of London. Series B: Biological Sciences*, **333**, 315–328.

GAUDANT, J. 2015. Présence du genre *Lepidocottus* Sauvage, 1875 (Teleostei, Gobioidei) dans l'Oligocène inférieur des environs de Céreste (Alpes-de-Haute-Provence, France). Geodiversitas, **37,** 229–235.

HAMMER, Ø., HARPER, D. A. T. and RYAN, P. D. 2001. PAST: Paleontological statistics software package for education and data analysis. *Palaeontologica Electronica*, **4**, 9.

HONG, L. and SIMON, J. D. 2006. Insight into the binding of divalent cations to *Sepia* eumelanin from IR absorption spectroscopy. *Photochemistry and Photobiology*, **82**, 1265–1269.

——— ——— 2007. Current understanding of the binding site, capacity, affinity, and biological significance of metals in melanin. *Journal of Physical Chemistry B,* **111**, 7938–7947.

HONG, L., LIU, Y. and SIMON, J. D. 2004. Binding of metal ions to melanin and their effects on the aerobic reactivity. *Photochemistry and Photobiology*, **80**, 477–481.

ITO, S., WAKAMATSU, K., GLASS, K., SIMON, J.D. 2013. High-performance liquid chromatography estimation of cross-linking of dihydroxyindole moiety in eumelanin. *Analytical Biochemistry,* **434**, 221–225.

LINDGREN, J., UVDAL, P., SJÖVDALL, P., NILSSON, D. E., ENGDAHL, A., SCHULTZ, B. P. and THIEL, V. 2012. Molecular preservation of the pigment melanin in fossil melanosomes**.** *Nature Communications,* **3**, 824.

LIU, Y., HONG, L., WAKAMATSU, K., ITO, S., ADHYARU, B., CHENG, C. Y., BOWERS, C. R., and SIMON, J. D. 2005. Comparison of structural and chemical properties of black and red human hair melanosomes. *Photochemistry and Photobiology,* **18**, 135–144.

LIU, Y., HONG, L., KEMPF, V. R., WAKAMATSU, K., ITO, S. and SIMON, J. D. 2004. Ion-exchange and adsorption of Fe(III) by *Sepia* melanin. *Pigment Cell Research*, **17**, 262–269.

LOEWEN, M. A., and BUCHHEIM, H. P. 1998. Paleontology and paleoecology of the culminating phase of Eocene fossil lake, Fossil Butte National Monument, Wyoming. *National Park Service Paleontological Research Volume* **3**, 73-80.

MANNING, P. L., EDWARDS, N. P., BERGMAN, U., ANNE, J., SELLERS, W. I., VAN VEELEN, A., SOKARAS, D., EGERTON, V. M., ALONSO-MORI, R., IGNATYEV, K.,

VAN DONGEN, B. E., WAKAMATSU, K., ITO, S., KNOLL, F., and WOGELIUS, R. A. 2019. Pheomelanin pigment remnants mapped in fossils of an extinct mammal. *Nature Communications*, **10**, 2250.

MCNAMARA, M. E., BRIGGS, D. E. G., ORR, P. J., FIELD, D. J. and WANG, Z. 2013. Experimental maturation of feathers: implications for reconstructions of fossil feather colour. *Biology Letters*, **9**, 20130184.

——— VAN DONGEN, B. E., LOCKYEAR, N. P., BULL, I. D. and ORR, P. J. 2016. Fossilization of melanosomes via sulfurization. *Palaeontology*, **59**, 337–350.

NAPPI, A. J. and CHRISTENSEN, B. M. 2005. Melanogenesis and associated cytotoxic reactions: Applications to insect innate immunity. *Insect Biochemistry and Molecular Biology*, **35**, 443–459.

OAKLEY, T. H. and SPEISER, D. I. 2015. How complexity originates: the evolution of animal eyes. *Annual Review of Ecology, Evolution and Systematics*, **46**, 237–260.

PEDERSEN, G. K. and BUCHARDT, B. 1996. The calcareous concretions (cementsten) in the Fur Formation (Paleogene, Denmark): isotopic evidence of early diagenetic growth. *Bulletin of the Geological Society of Denmark*, **43,** 78–86.

RAVEL, B. and NEWVILLE, M. 2005. Athena, Artemis, Hephaestus: data analysis for X-ray absorption spectroscopy using IFEFFIT. *Journal of Synchrotron Radiation*, **12**, 537–541.

ROGERS, C. S., ASTROP, T. I., MCNAMARA, M. E., WEBB, S. M., ITO, S. and WAKAMATSU, K. 2019. Synchrotron-X-ray absorption spectroscopy of melanosomes in vertebrates and cephalopods: implications for the affinity of *Tullimonstrum*. *Proceedings of the Royal Society B*, **286**, 20191649.

———, WEBB, S. M. and MCNAMARA, M. E. 2020. Data from: Synchrotron-X-ray fluorescence analysis reveals diagenetic alteration of fossil melanosome trace metal chemistry. *Dryad Digital Repository*. https://datadryad.org/stash/share/XXXX

ROSSI, V., MCNAMARA, M. E., WEBB, S. M., ITO, S. and WAKAMATSU, K. 2019. Tissue-specific geometry and chemistry of modern and fossilized melanosomes reveal internal anatomy of extinct vertebrates. *Proceedings of the National Academy of Sciences USA*, **116**, 17880–17889.

———, WEBB, S.M. and MCNAMARA, M.E. 2020. Hierarchical biota-level and taxonomic controls on the chemistry of fossil melanosomes revealed using synchrotron X-ray fluorescence. *Scientific Reports*, **10**, 8970.

SCHROETER, E. R., DeHART, C. J. CLELAND, T.P., ZHENG, W., THOMAS, P. M., KELLEHER, N. L., BERN, M. and SCHWEITZER, M. H. 2017. Expansion for the *Brachylophosaurus canadensis* collagen I sequence and additional evidence of the preservation of Cretaceous protein. *Journal of Proteome Research*, **16**, 920–932.

SCHWEITZER, M. H., SUO, Z., RECEP, A., ASARA, J. M., ALLEN, M. A., ARCE, F. T., and HORNER, J. R. 2007. Analysis of soft tissue from *Tyrannosaurus rex* suggests the presence of protein. *Science*, **316**, 277–280.

———, ZHENG, W., CLELAND, T.P. and BERN, M. 2013. Molecular analyses of dinosaur osteocytes support the presence of endogenous molecules. *Bone*, **52**, 414–423.

STANKIEWICZ, A. R., BRIGGS, D. E. G., MICHELS, R., COLLINSON, M. E., FLANNERY, M. B. and EVERSHED, R. P. 2000. Alternative origin of aliphatic polymer in kerogen. *Geology*, **28**, 559–562.

543 WEBB, S. M. 2011. The microanalysis toolkit: X-ray fluorescence image processing
544 software. *AIP Conference Proceedings*, **1365**, 196–199.

545 WOGELIUS, R. A., MANNING, P. L., BARDEN, H. E., EDWARDS, N. P., WEBB, S. M.,
546 SELLERS, W. I., TAYLOR, K. G., LARSON, P. L., DODSON, P., YOU, H., DA-QING,
547 L. and BERGMANN, U. 2011. Trace metals as biomarkers for eumelanin pigment in the
548 fossil record. *Science*, **333**, 1622–1626.

549

550 **Figure captions:**

551 **Figure 1.** Effect of temperature and pressure on the trace element chemistry of eye
552 melanosomes of *Dicentrarchus* (Actinopterygii: Perciformes). A, Linear Discriminant
553 Analysis chemospace plot based on measured concentrations of Ca, Fe, Cu and Zn in
554 untreated and experimentally matured melanosomes. B, Biplot showing the contribution of
555 each element to variation in A.

556 **Figure 2.** Differences in the concentrations of key elements Ca, Fe, Cu and Zn in
557 melanosome extracts from eyes of *Dicentrarchus*. X-axis labels refer to untreated extracts
558 (UNMAT) and extracts matured under various conditions as follows: Cu T only, Cu-solution
559 with elevated temperature; Cu T&P, Cu-solution with elevated temperature and pressure; Cu
560 & Zn, Cu-Zn-solution with elevated temperature and pressure; DD T only, distilled water
561 with elevated temperature; DD T&P, distilled water with elevated temperature and pressure;
562 Zn, Zn-solution with elevated temperature and pressure; UNMAT, untreated melanosomes.
563 Concentration units are $\mu g/cm^2$.

564 **Figure 3.** Comparison of the trace element chemistry of melanosome extracts and fossil
565 melanosomes. A, Linear Discriminant Analysis chemospace plot including data for Ca, Fe,

Cu and Zn in unmatured and matured melanin extracts from eye melanosomes of *Dicentrarchus* and from fossil Teleostei (*Dapalis, Knightia* and Tetradontiformes). B, Biplot of key elements and their contribution to variation in A. C, XANES spectra at the Cu K edge at 8987 eV (dashed line).

Figure 4. A, Comparison of data on Zn and B, log Zn and Cu chemistry concentrations and log Zn:Cu ratios among matured and unmatured melanosome extracts and fossil eyespot melanins. X-axis labels refer to fossil specimens, untreated extracts (UNMAT) and extracts matured under various conditions as follows Cu T only, Cu-solution with elevated temperature; Cu T&P, Cu-solution with elevated temperature and pressure; Cu & Zn, Cu-Zn-solution with elevated temperature and pressure; DD T only, distilled water with elevated temperature; DD T&P, distilled water with elevated temperature and pressure; Zn, Zn-solution with elevated temperature and pressure; UNMAT, untreated melanosomes. Data from Mazon Creek (MC) vertebrates, Tetradontiformes and *Knighita* are from Rogers *et al.* 2019. Concentration units are $\mu g/cm^2$.

Figure 1.

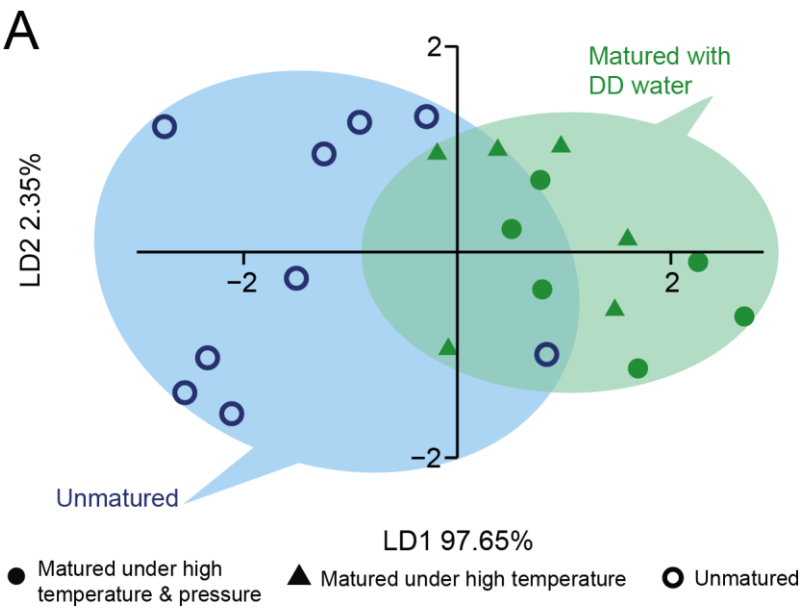
A
Matured with
DD water
Unmatured
LD2 2.35%
LD1 97.65%
2
−2
−2
2
Matured under high
temperature & pressure
Matured under high temperature
Unmatured

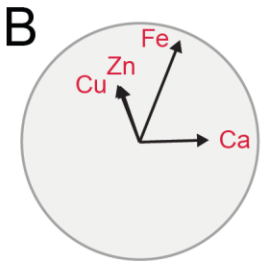
B
Fe
Zn
Cu
Ca

584 **Figure 2.**

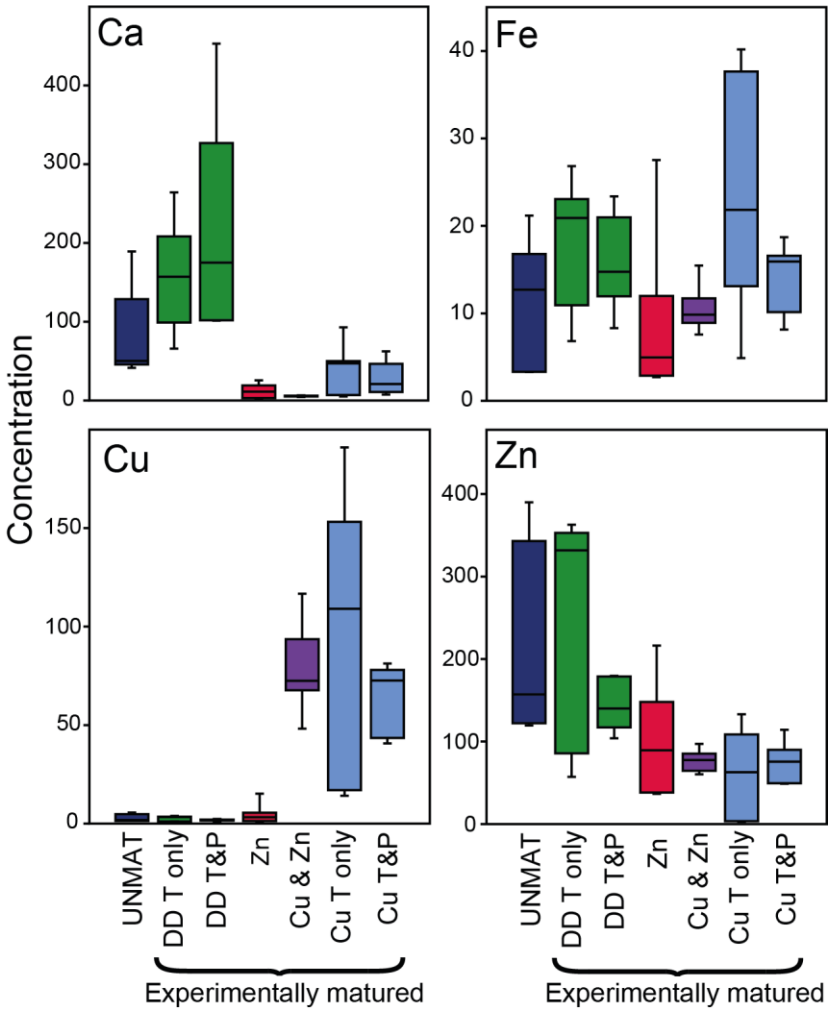

585

586

Figure 3.

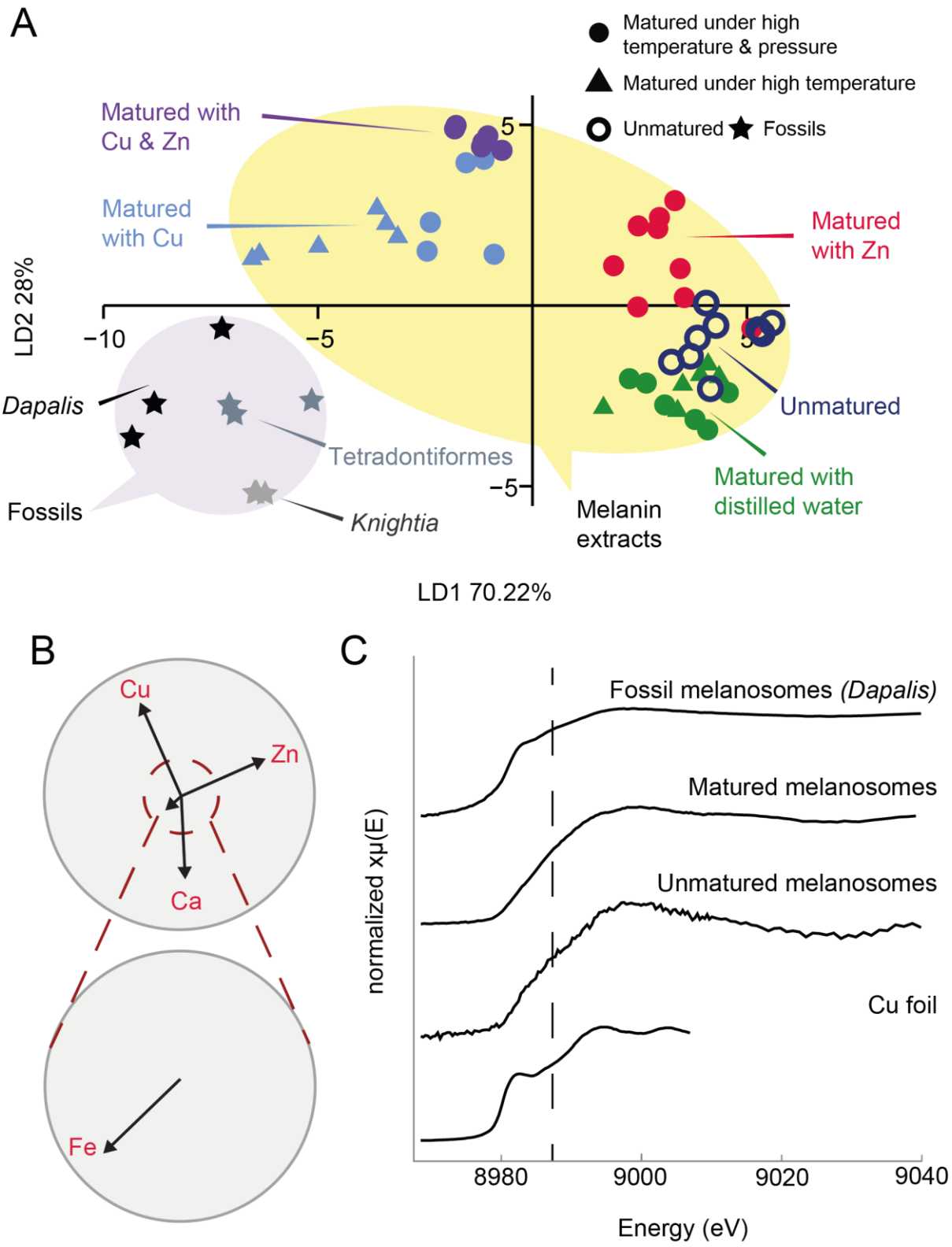
A
Matured under high temperature & pressure
Matured under high temperature
Unmatured
Fossils
Matured with Cu & Zn
Matured with Cu
Matured with Zn
Unmatured
Matured with distilled water
Melanin extracts
Dapalis
Tetradontiformes
Knightia
Fossils
LD2 28%
LD1 70.22%
−10
−5
5
−5
B
Cu
Zn
Ca
Fe
C
Fossil melanosomes (Dapalis)
Matured melanosomes
Unmatured melanosomes
Cu foil
normalized xμ(E)
8980
9000
9020
9040
Energy (eV)

590 **Figure 4.**

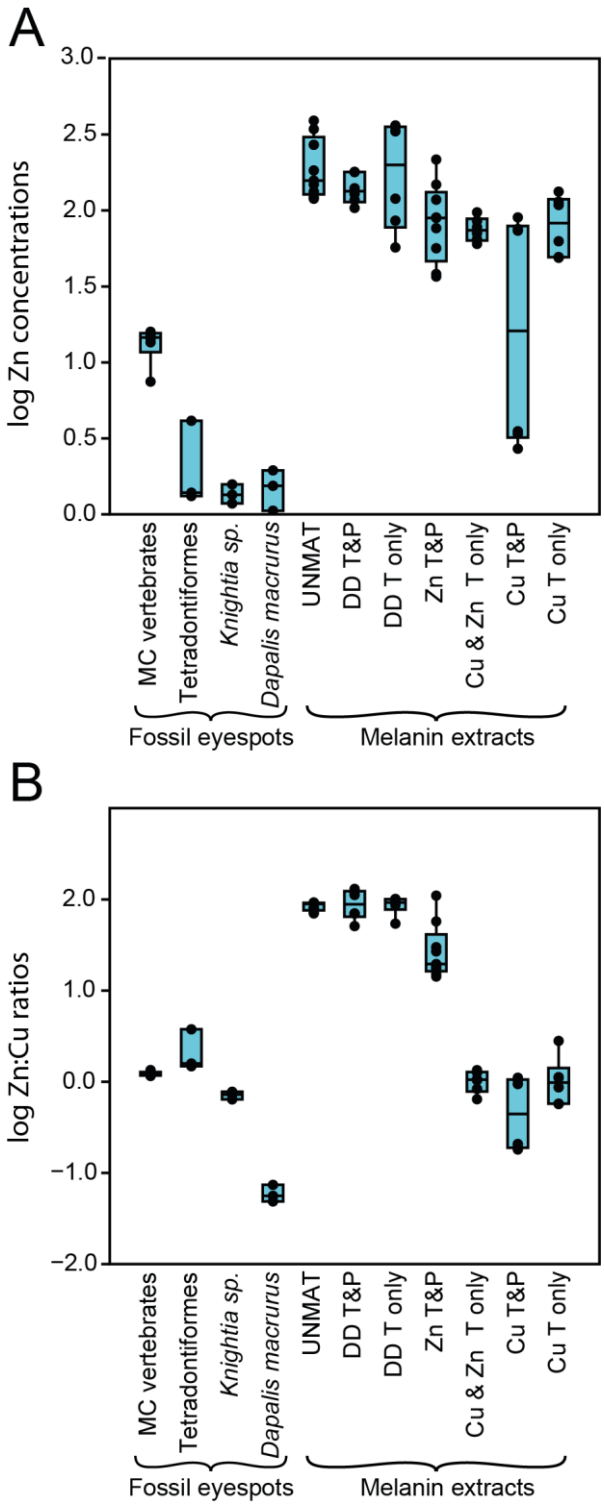

591

Supplementary Information for

Synchrotron-X-ray fluorescence analysis reveals diagenetic alteration of fossil melanosome trace metal chemistry

Christopher S. Rogers, Maria E. McNamara, Samuel M. Webb

Christopher S. Rogers, Maria E. McNamara

Email: christopher.rogers@ucc.ie; maria.mcnamara@ucc.ie

This PDF file includes:

Figures S1 to S9

Tables S1 to S5

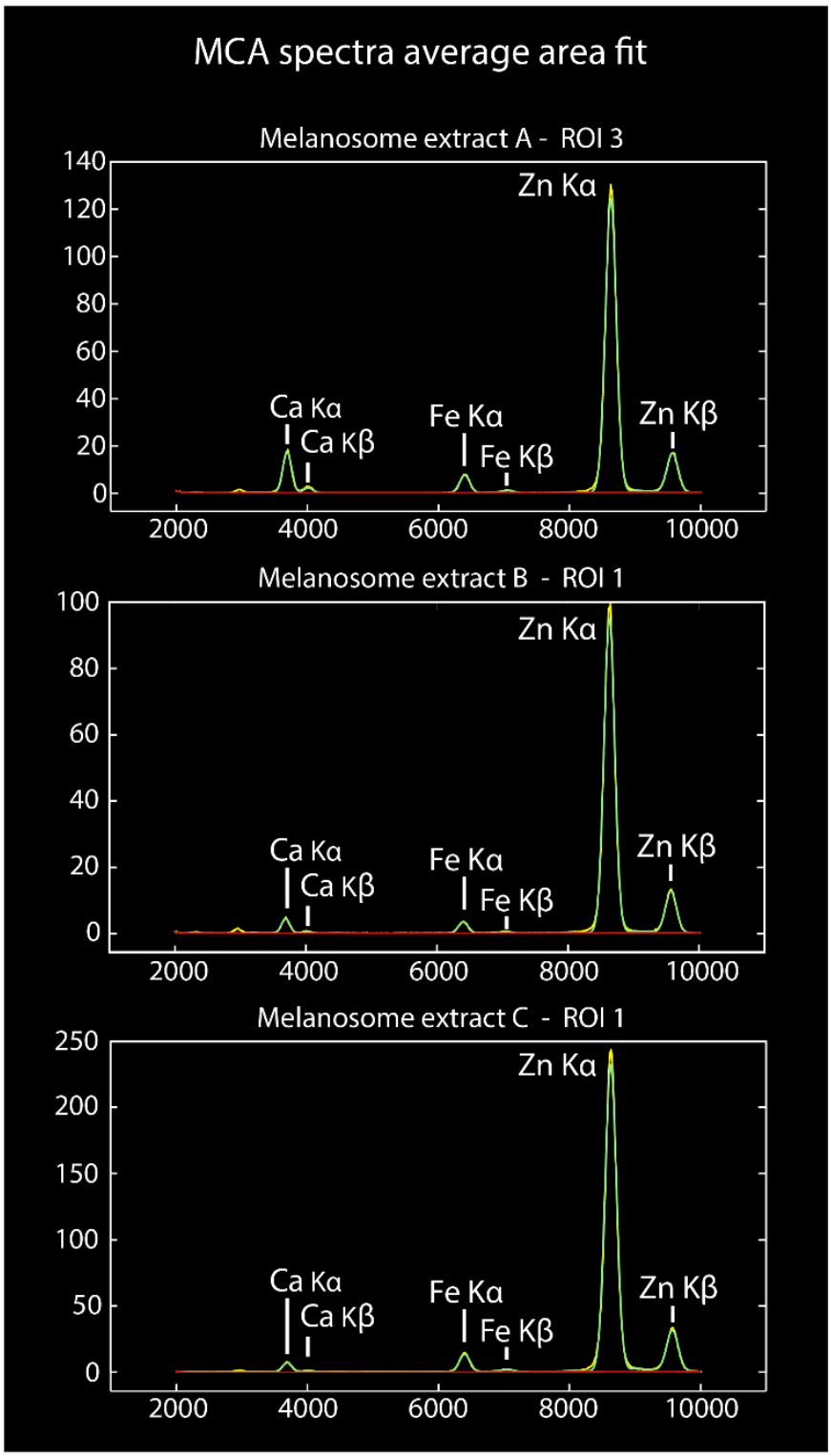

Fig. S1. MCA spectra from regions of interest in SRS-XRF maps of unmatured melanin extracts A–C. X-axis, X-ray emission energy (keV). Y-axis, counts. Yellow line denotes measured data; green line denotes the computed fit.

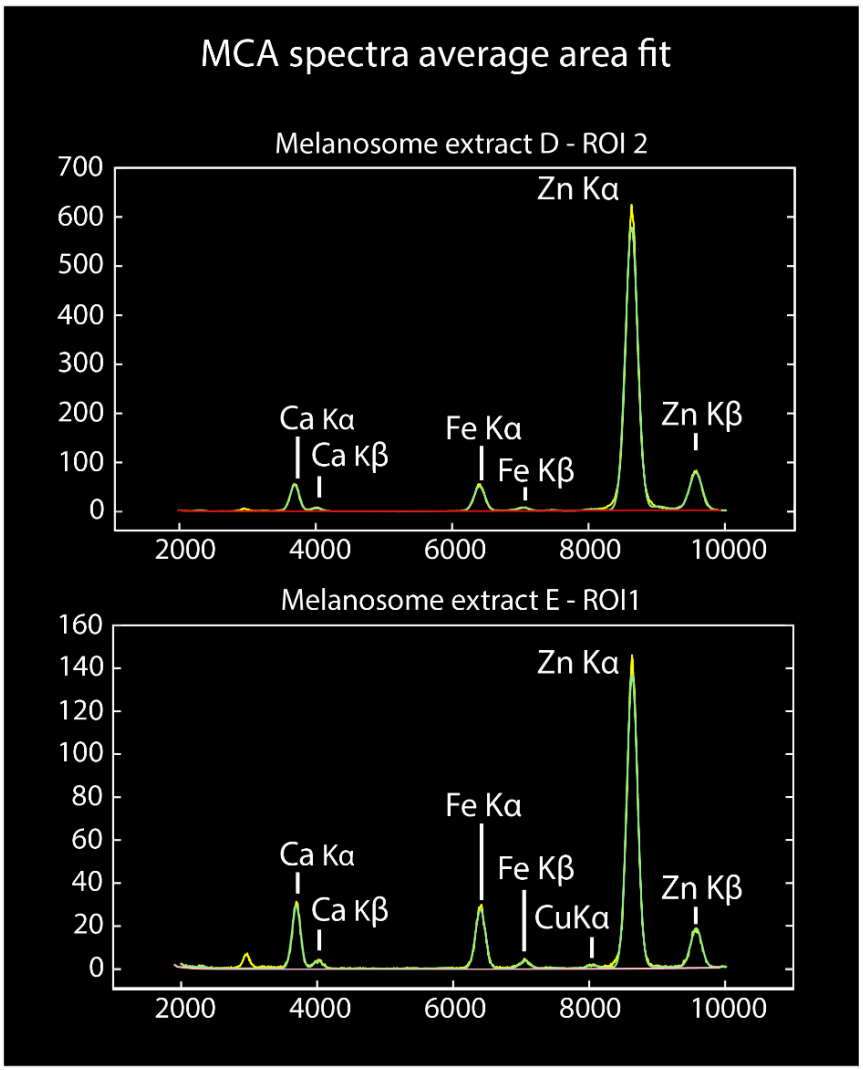

Fig. S2. MCA spectra from regions of interest in SRS-XRF maps of unmatured melanin extracts D, E. X-axis, X-ray emission energy (keV). Y-axis, counts. Yellow line denotes measured data; green line denotes the computed fit.

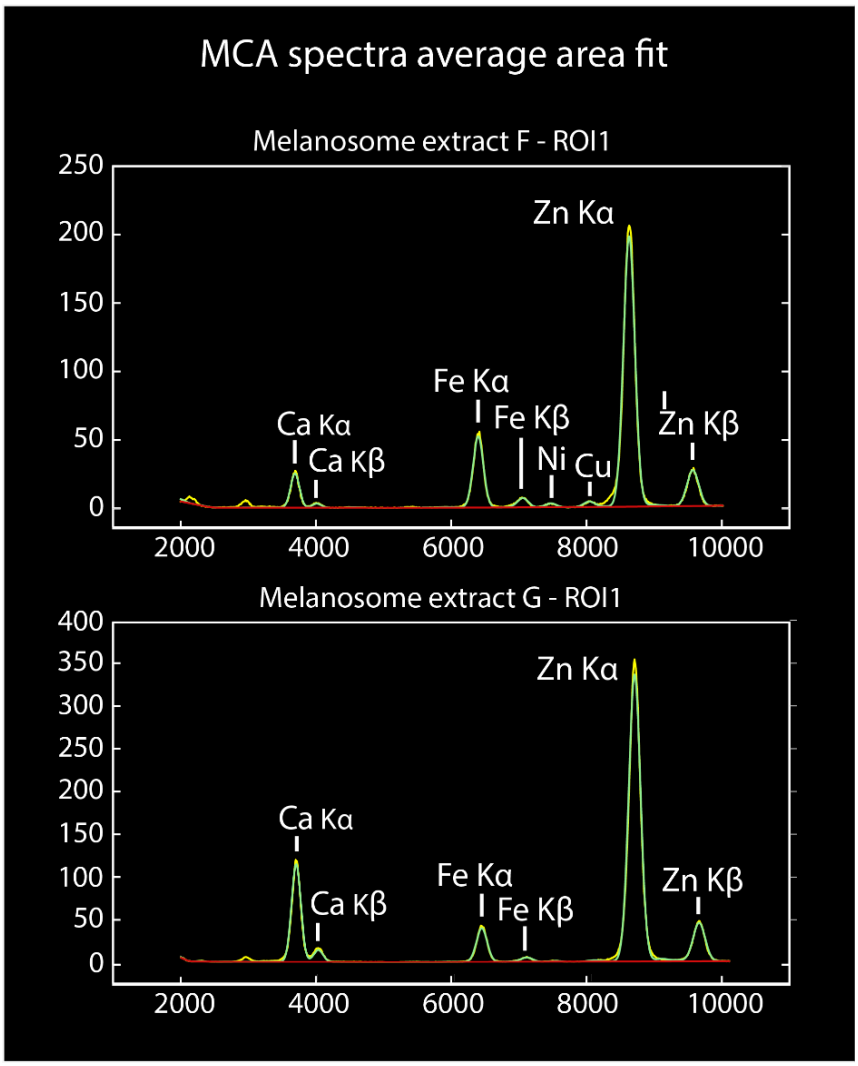

Fig. S3. MCA spectra from regions of interest in SRS-XRF maps of unmatured melanin extracts F, G. X-axis, X-ray emission energy (keV). Y-axis, counts. Yellow line denotes measured data; green line denotes the computed fit.

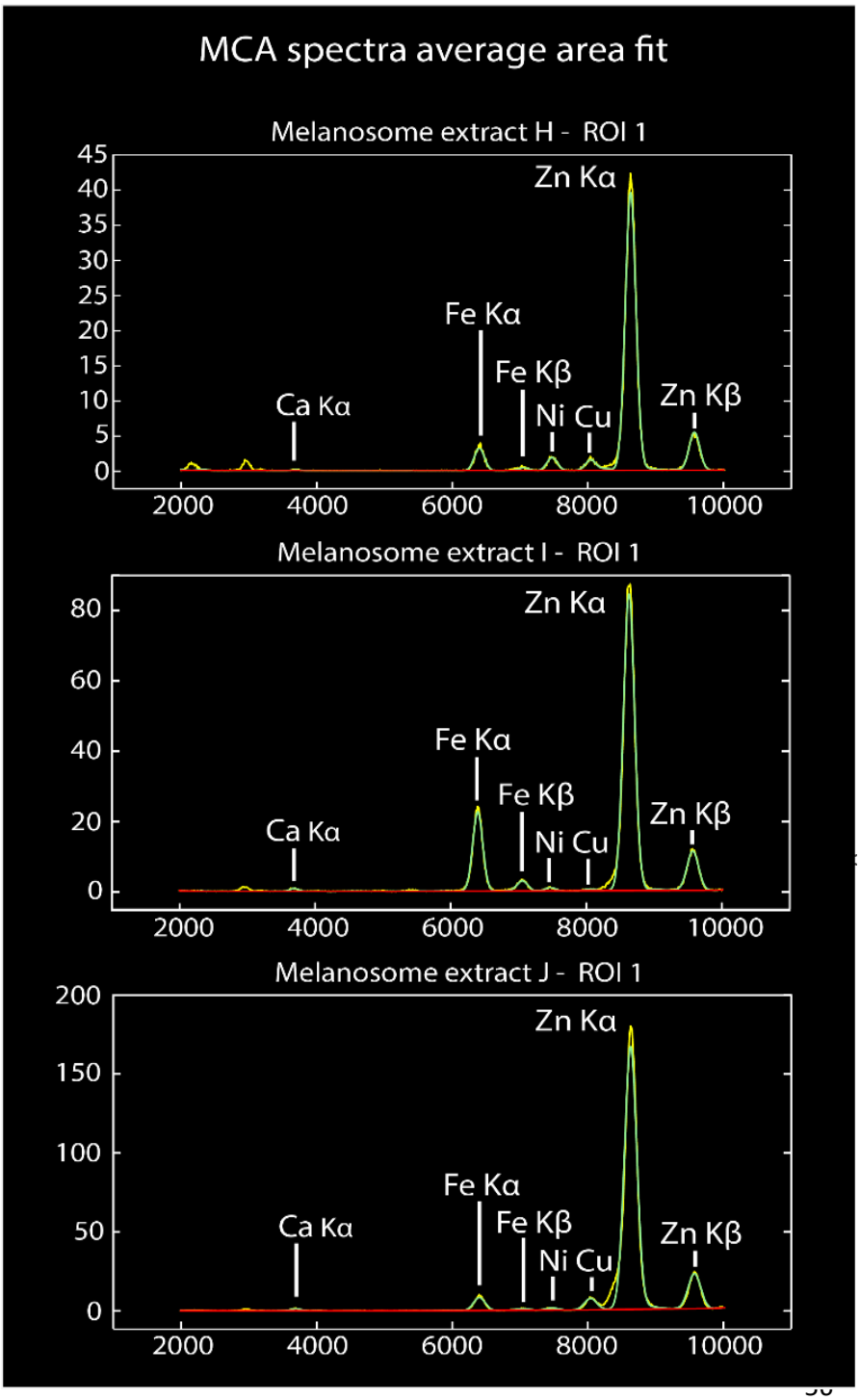

Figure S4. MCA spectra from regions of interest in SRS-XRF maps of unmatured melanin extracts H, I, J. X-axis, X-ray emission energy (keV). Y-axis, counts. Yellow line denotes measured data; green line denotes the computed fit.

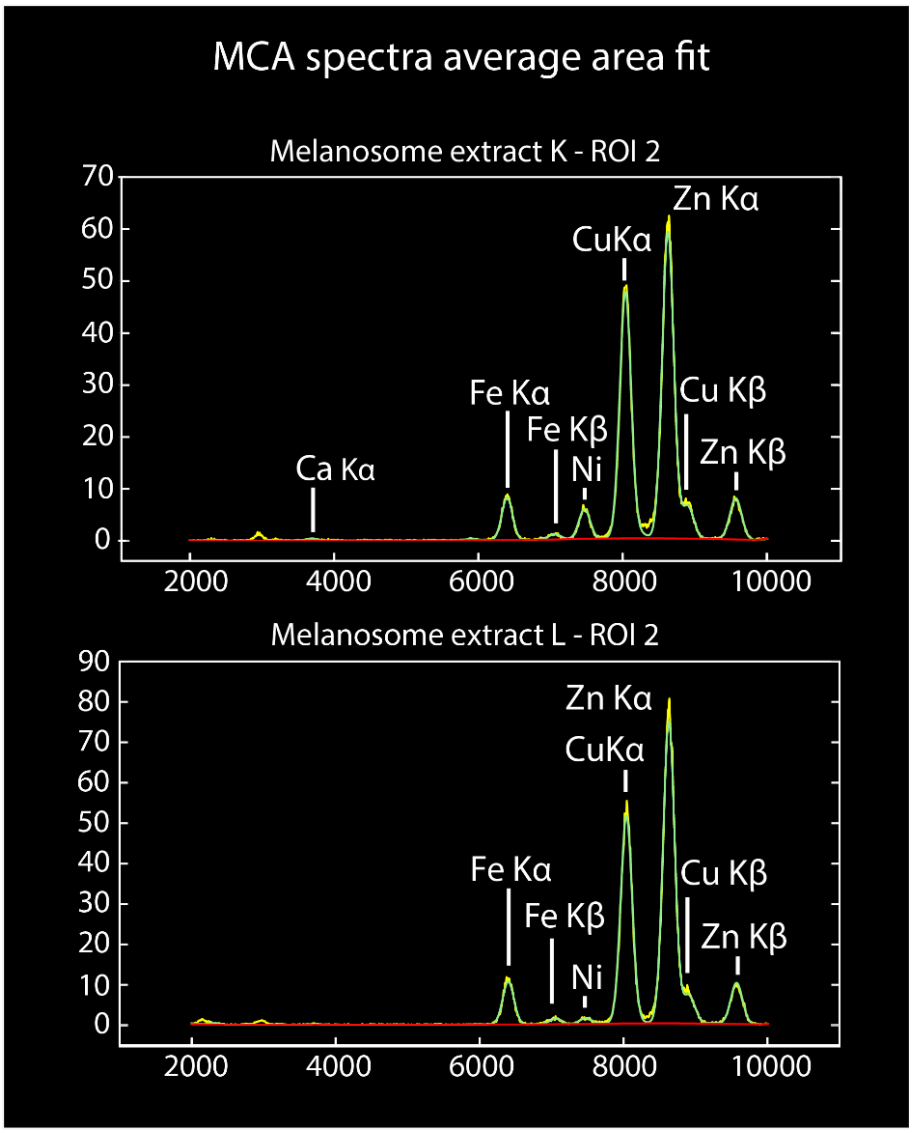

Fig. S5. MCA spectra from regions of interest in SRS-XRF maps of unmatured melanin extracts K, L. X-axis, X-ray emission energy (keV). Y-axis, counts. Yellow line denotes measured data; green line denotes the computed fit.

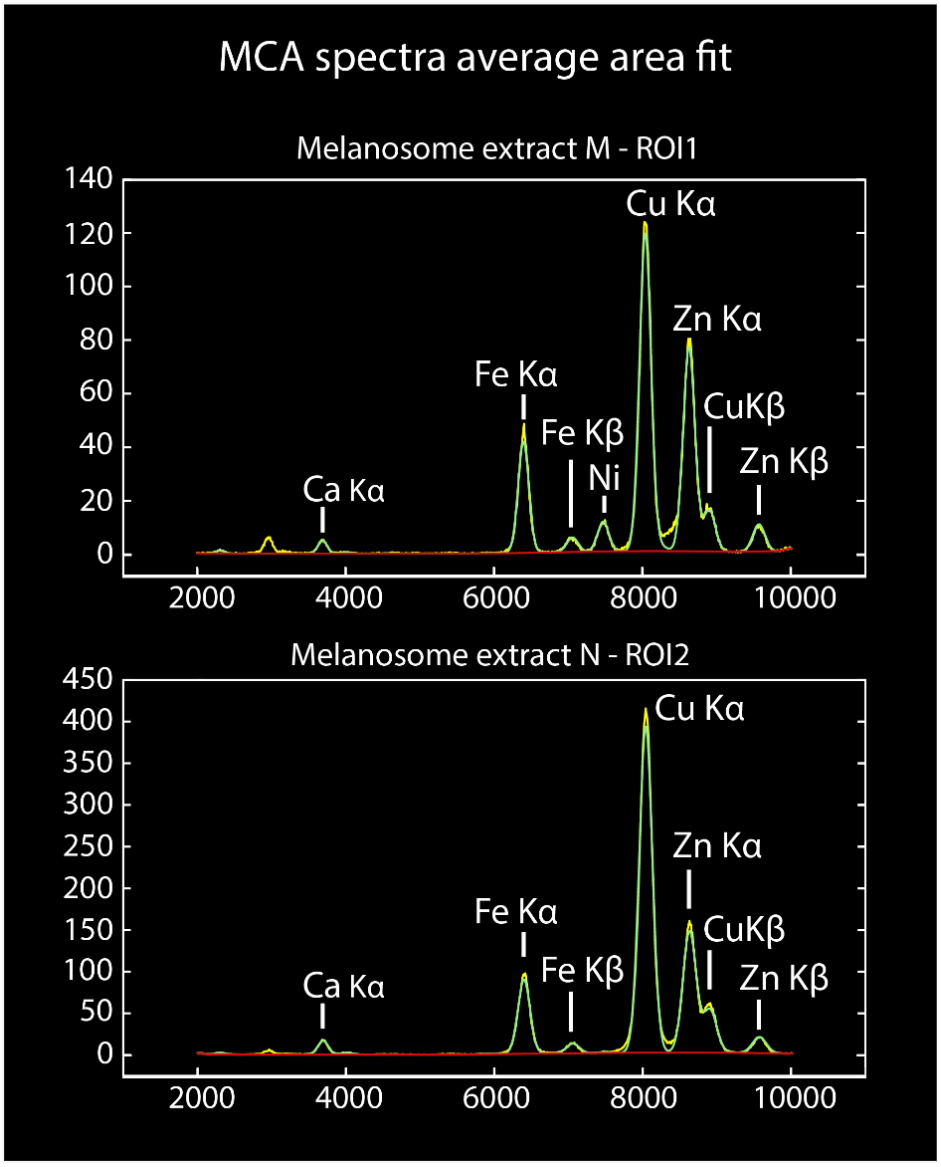

Fig. S6. MCA spectra from regions of interest in SRS-XRF maps of unmatured melanin extracts M, N. X-axis, X-ray emission energy (keV). Y-axis, counts. Yellow line denotes measured data; green line denotes the computed fit.

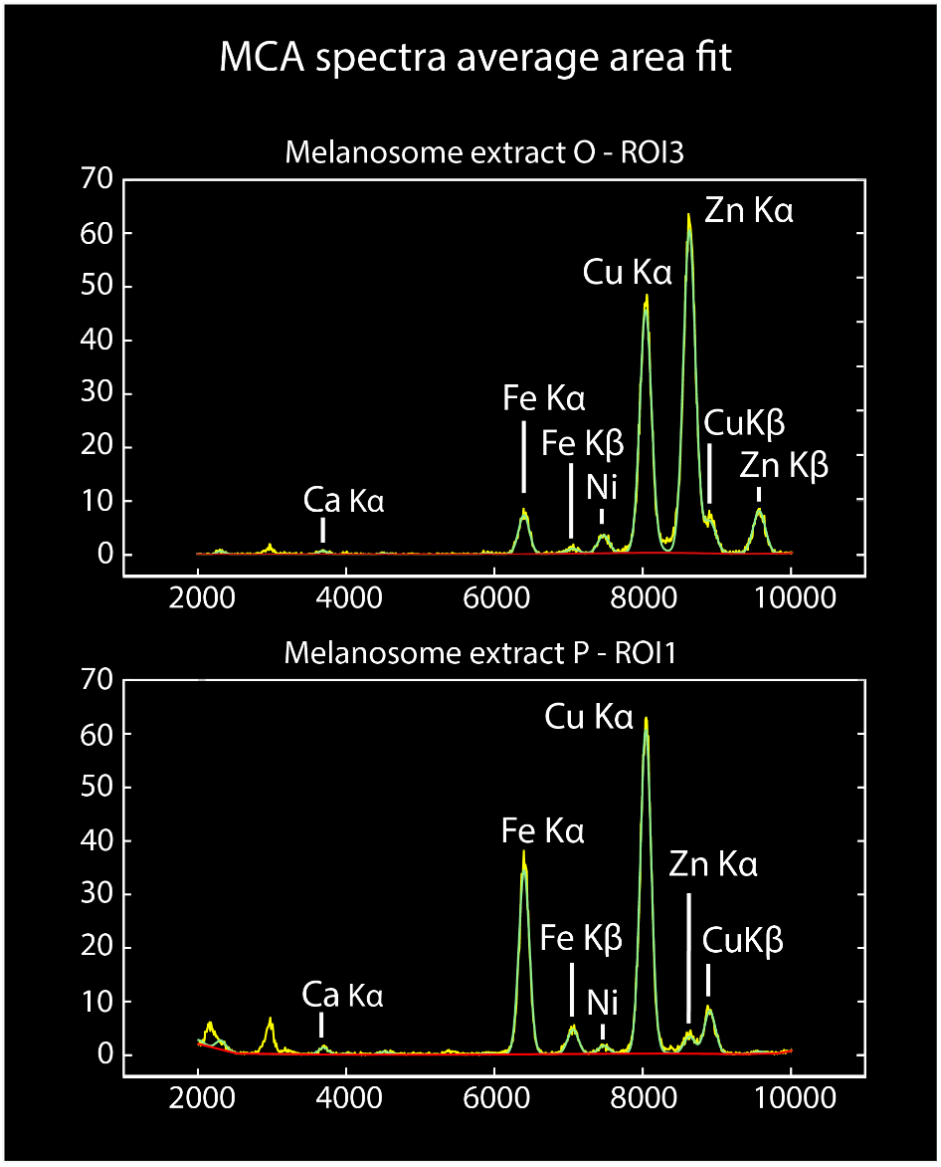

Fig. S7. MCA spectra from regions of interest in SRS-XRF maps of unmatured melanin extracts O, P. X-axis, X-ray emission energy (keV). Y-axis, counts. Yellow line denotes measured data; green line denotes the computed fit.

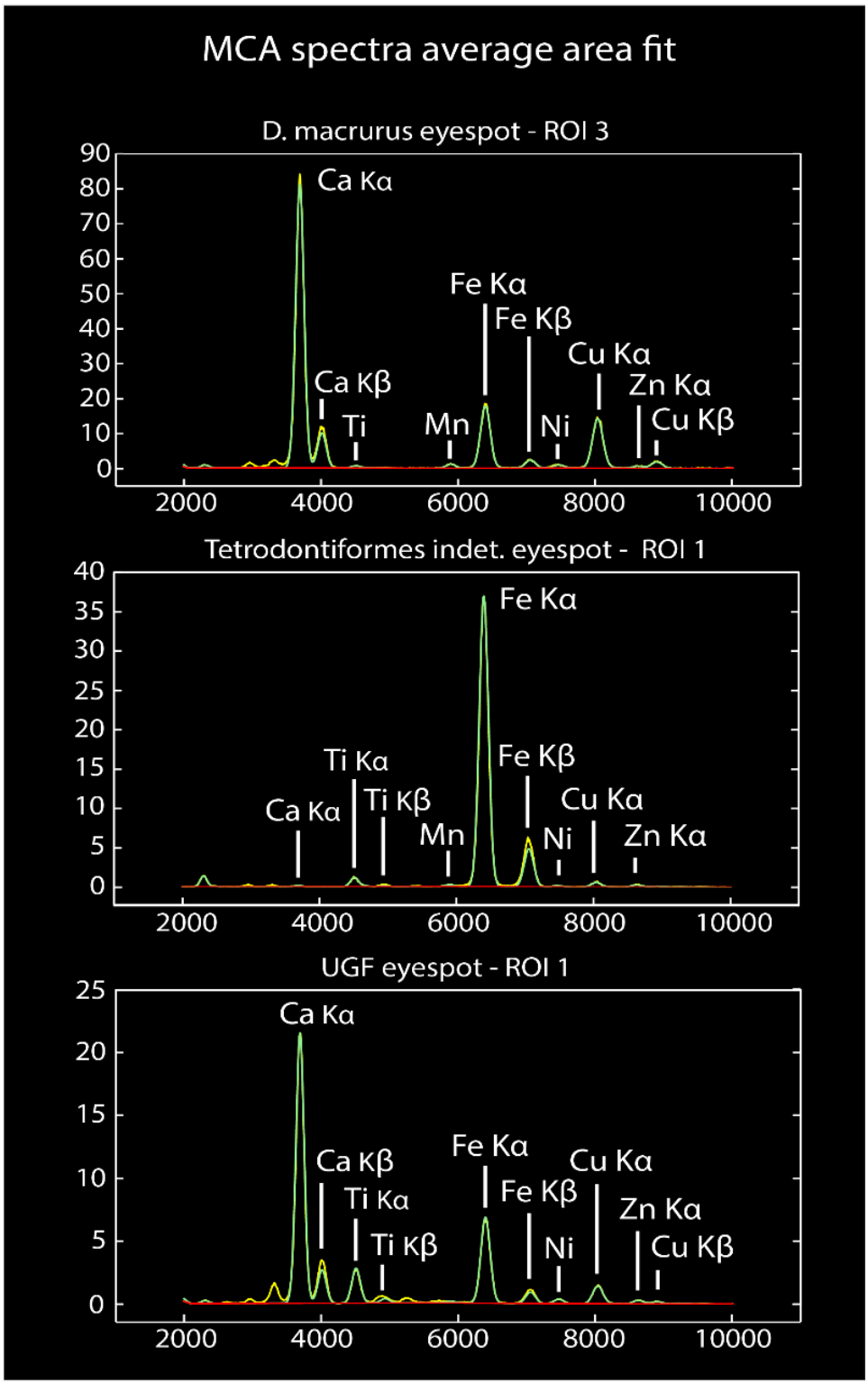

Fig. S8. MCA spectra from regions of interest in SRS-XRF maps of fossil eyespots of *D. macrurus*, NHMD 199838 (Tetrodontiformes indet.) and UGF 2015-16 X-axis, X-ray emission energy (keV). Y-axis, counts. Yellow line denotes measured data; green line denotes the computed fit.

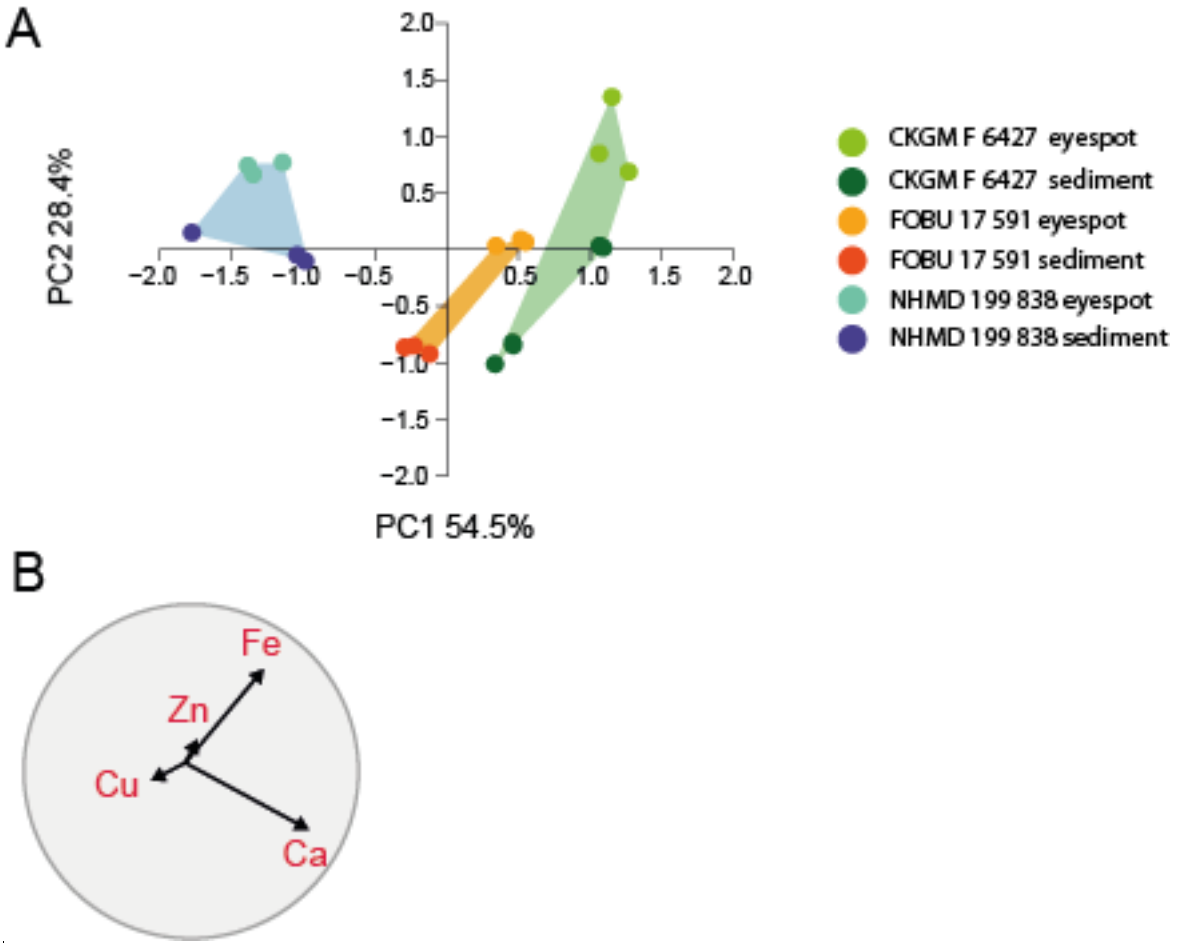

Fig. S9. A, principal Components Analysis of chemical data for fossil melanosomes from CKGM F 6427 (*Dapalis macrurus*), FOBU 17 591 (*Knightia*) and NHMD 199 838 (Tetradontiformes indet.). B, Biplot of key elements and their contribution to variation in A. The analyses used data for Ca, Fe, Cu and Zn only.

Table S1. List of maturation treatments.

Melanosome extracts	Experimental maturation treatment
A-C	Unmatured
D-E	Matured in DD water, with elevated temperature only
F-G	Matured in DD water, with elevated temperature and pressure
H-J	Matured in Zn, with elevated temperature and pressure
K-L	Matured in Cu and Zn, with elevated temperature and pressure
M-N	Matured in Cu, with elevated temperature only
O-P	Matured in Cu, with elevated temperature and pressure

Table S2. Statistical analyses of trace element concentrations in melanosome extracts. A, ANOVA / Welch's F-test (*); B, Kruskal-Wallis; C, Post-hoc analyses for Welch F test and Kruskal-Wallis (Dunn's post hoc). Cu T only, extract with added Cu-rich solution treated to elevated temperature; Cu T&P, extract with added Cu-rich solution treated to elevated temperature and pressure; Cu & Zn, extract with added Cu-and Zn-rich solution treated to elevated temperature and pressure; DD T only, extract with added distilled water treated to elevated temperature; DD T&P, extract with added distilled water treated to elevated temperature and pressure; Zn, extract with added Zn-rich solution treated t elevated temperature and pressure; UNMAT, untreated melanosomes. † indicates concentration data that were log-transformed prior to statistical testing to make the data conform to normality.

A

Element concentration	df	F	p
Fe	2.115†	17.5†	0.1034†
Ca	16.18*†	73.39*†	7.91 E-11*†
Cu	17.47*†	118.8*†	5.792 E-13*†

B

Element concentration	H (chi^2)	p
Zn	23.33	0.000693

C

Ca

	UNMAT	DD T only	DD T & P	Zn	Cu & Zn	Cu T & P	Cu T only
UNMAT		2.43E-01	1.57E-01	4.44E-03	1.03E-03	1.23E-01	1.12E-01
DD T only	2.43E-01		8.21E-01	2.06E-04	4.86E-05	1.34E-02	1.19E-02
DD T & P	1.57E-01	8.21E-01		7.48E-05	1.80E-05	6.91E-03	6.10E-03
Zn	4.44E-03	2.06E-04	7.48E-05		4.61E-01	3.17E-01	3.39E-01
Cu & Zn	1.03E-03	4.86E-05	1.80E-05	4.61E-01		1.12E-01	1.22E-01
Cu T & P	1.23E-01	1.34E-02	6.91E-03	3.17E-01	1.12E-01		9.67E-01
Cu T only	1.12E-01	1.19E-02	6.10E-03	3.39E-01	1.22E-01	9.67E-01	

Cu

	UNMAT	DD T only	DD T & P	Zn	Cu & Zn	Cu T & P	Cu T only
UNMAT		7.07E-01	5.32E-01	6.49E-01	8.75E-04	2.41E-03	1.78E-03
DD T only	7.07E-01		8.21E-01	4.34E-01	7.21E-04	1.85E-03	1.39E-03
DD T & P	5.32E-01	8.21E-01		3.02E-01	3.08E-04	8.37E-04	6.20E-04
Zn	6.49E-01	4.34E-01	3.02E-01		3.49E-03	8.60E-03	6.57E-03
Cu & Zn	8.75E-04	7.21E-04	3.08E-04	3.49E-03		7.89E-01	8.53E-01
Cu T & P	2.41E-03	1.85E-03	8.37E-04	8.60E-03	7.89E-01		9.34E-01
Cu T only	1.78E-03	1.39E-03	6.20E-04	6.57E-03	8.53E-01	9.34E-01	

	UNMAT	DD T only	DD T & P	Zn	Cu & Zn	Cu T & P	Cu T only

Zn	UNMAT		7.68E-01	1.75E-01	6.19E-03	1.79E-03	1.79E-03	5.61E-03
	DD T only	7.68E-01		8.10E-01	1.12E-01	9.27E-02	6.56E-02	6.56E-02
	DD T & P	1.75E-01	8.10E-01		8.75E-02	5.08E-03	8.24E-03	3.06E-02
	Zn	6.19E-03	1.12E-01	8.75E-02		6.80E-01	5.96E-01	2.16E-01
	Cu & Zn	1.79E-03	9.27E-02	5.08E-03	6.80E-01		9.36E-01	4.71E-01
	Cu T & P	1.79E-03	6.56E-02	8.24E-03	5.96E-01	9.36E-01		4.71E-01
	Cu T only	5.61E-03	6.56E-02	3.06E-02	2.16E-01	4.71E-01	4.71E-01	

Table S3. Statistical analyses of trace element concentrations in fossil eyespots. A, Welch's ANOVA; B, Kruskal-Wallis test; C, Dunn's post hoc analyses for both Welch's ANOVA and Kruskal-Wallis. † indicates concentration data that were log-transformed prior to statistical testing due to non-normality.

A

Element concentration	df	F	p
Ca	2.668	37.62	0.01109
Fe	8†	162†	0.03136†
Cu	2.983†	13.7†	0.8371†

B

Element concentration	H (chi^2)	p
Zn	0.3556	0.8371

C

		CKGM F 6327	FOBU 17 591	NHMD 199838
Ca	CKGM F 6327		0.8815	0.05263
	FOBU 17 591	0.8815		0.03689
	NHMD 199838	0.05263	0.03689	

		CKGM F 6327	FOBU 17 591	NHMD 199838
Fe	CKGM F 6327		0.8815	0.03689
	FOBU 17 591	0.8815		0.05263
	NHMD 199838	0.03689	0.05263	

		CKGM F 6327	FOBU 17 591	NHMD 199838
Cu	CKGM F 6327		0.1797	0.00729
	FOBU 17 591	0.1797		0.1797
	NHMD 199838	0.00729	0.1797	

Table S4. Statistical analyses of trace element concentrations between fossil eyespots and associated sedimentary matrix. A, t-test; B, Welch's F-test; C, Mann Whitney-U. † indicates concentration data that were log-transformed prior to statistical testing due to non-normality.

A

Element concentration	Specimen	df	t	p
Ca	CKGM F 6327	6	3.9178	0.0078
	FOBU 17 591	4	0.0813	0.93913
Fe	CKGM F 6327 †	6†	3.2465†	0.0228†
Cu	NHMD 199838†	4†	7.0917†	0.0020877†
Zn	FOBU 17 591	4	0.0308	0.96693
	NHMD 199838	4	1.454	0.21963

B

Element concentration	Specimen	df	F	p
Ca	NHMD 199838	2.043	3.073	0.219
Fe	FOBU 17 591	2.07	106	0.008268
	NHMD 199838	2.062	0.6704	0.4967
Cu	CKGM F 6327†	2.004†	2.07†	0.01327†
	FOBU 17 591	2.07	0.0813	0.93913

C

Element concentration	Specimen	df	U	p
Zn	CKGM F 6327	1875, 2.625	6	0.21963

Table S5. Statistical analyses of differences between the trace element concentrations in unmatured melanosome extracts and fossils. A, ANOVA; B, Kruskal-Wallis. † indicates concentration data that were log-transformed prior to statistical testing due to non-normality.

A

Element concentration	df	F	p
Fe	17†	3.478†	0.08063†

B

Element concentration	H (chi^2)	p
Ca	1.421	0.2332
Cu	0.001949	0.9648
Zn	12.79	0.000349